Molecular beam epitaxial growth of IV–VI multiple quantum well structures on Si(111) and BaF_2(111) and optical studies of epilayer heating

H. Z. Wu,[a] P. J. McCann, O. Alkhouli, X. M. Fang,[b] D. McAlister,[c] and K. Namjou[d]
School of Electrical and Computer Engineering and Laboratory for Electronic Properties of Materials, University of Oklahoma, Norman, Oklahoma 73019

N. Dai and S. J. Chung
Department of Physics and Astronomy and Laboratory for Electronic Properties of Materials, University of Oklahoma, Norman, Oklahoma 73019

P. H. O. Rappl
Instituto Nacional de Pesquisas Espaciais- INPE; CP 515 12201-970 São José dos Campos, SP, Brazil

(Received 28 December 2000; accepted 21 May 2001)

IV–VI semiconductor multiple quantum well (MQW) structures (PbSe/PbSrSe) were grown on Si(111) and BaF_2(111) substrates by molecular beam epitaxy. Structural and optical properties of the MQW structures have been studied using reflection high-energy electron diffraction, high resolution x-ray diffraction (HRXRD), Fourier-transform infrared (FTIR) transmission, and midinfrared photoluminescence (PL). Numerous satellite diffraction peaks and narrow linewidths of the HRXRD rocking curves indicate the high crystalline quality of the structures grown on both Si and BaF_2. Longitudinal and oblique valley subband transitions without superposed interference fringes were observed in FTIR differential transmission spectra. Continuous wave midinfrared photoluminescence was also observed from both sets of samples. Comparison of FTIR and PL spectra allows determination of localized epilayer heating in the MQW samples due to optical pumping. For a typical laser pumping power of 9.1 W/cm^2 the heating in a MQW layer on Si(111) was 70 °C, while the amount of heating for a MQW layer on lower thermal conductivity BaF_2 was 83 °C. [DOI: 10.1116/1.1385915]

I. INTRODUCTION

A demonstration of above room temperature continuous wave midinfrared photoluminescence (PL) from a IV–VI semiconductor material was recently reported.[1] This achievement is believed to be due to the unique properties of the IV–VI semiconductor multiple quantum well (MQW) structures that were employed. These include nearly equal electron and hole effective masses and lack of valence band degeneracy, properties that enable strong electron-hole pair localization in quantum wells and reduction of nonradiative Auger recombination, respectively. Together, these effects significantly enhance radiative recombination at noncryogenic temperatures and allow light emission using low intensity pump sources such as unfocused diode lasers. PL characterization using diode laser pumping allows precise control of incident photon flux by changing diode laser pump current. Such characterization has created a way to investigate the properties of thin film IV–VI semiconductor materials. In this article, PbSe/PbSrSe MQW structures grown by molecular beam epitaxy (MBE) on both Si(111) and BaF_2(111) substrates are described and results from diode laser pumped PL spectroscopy experiments are reported. In addition, structural and electronic properties of these MQW structures obtained using reflection high-energy electron diffraction (RHEED), high-resolution x-ray diffraction (HRXRD), and Fourier-transform infrared (FTIR) transmission spectroscopy are reported. Results from these measurements have allowed accurate determination of localized heating in IV–VI semiconductor thin films due to optical pumping.

II. EXPERIMENTS

A. MBE growth procedures

PbSe/PbSrSe MQW structures were grown on both 3 in. diameter Si(111) and freshly cleaved 1 cm×1 cm BaF_2(111) substrates in an Intevac GEN II modular MBE system. The Si(111) substrates were cleaned using the modified Shiraki method followed by dipping in a dilute HF solution.[2] Si wafers and BaF_2 substrates were outgassed in the buffer chamber at 200 °C for 1 h before being transferred to the growth chamber. Auger spectroscopy analysis was performed on thermally cleaned Si(111) wafers. No carbon related Auger peaks were observed after the hydrogen-passivated layer was desorbed from the Si surface at temperatures of 540 °C. To accommodate the large lattice mismatch and thermal expansion coefficient difference between the Si substrate and PbSe/PbSrSe, a 20 Å CaF_2 buffer layer was directly grown on the silicon and a 600-nm-thick BaF_2 buffer layer was grown on the CaF_2 buffer layer. Both fluoride layers were grown at a substrate temperature of 700 °C. Substrate temperature was then reduced to 360 °C for growth of a 3-μm-thick PbSrSe buffer layer and the MQW structure. Each MQW structure consisted of 20–40 pairs of PbSe/PbSrSe

[a]Electronic mail: huizhen@ou.edu
[b]Present address: Quantum Epitaxial Designs, Inc., Bethlehem, PA.
[c]Present address: ON Semiconductor, Phoenix, AZ.
[d]Present address: Ekips Technologies, Norman, OK.

layers grown on top of the PbSrSe buffer layer. PbSe quantum-well and PbSrSe barrier layer thicknesses were in the range of 50–300 and 250–500 Å, respectively. A 3% Sr-to-PbSe flux ratio was used for the growth of the PbSrSe buffer layer and barrier layers, and, based on the work of Lambrecht *et al.*,[3] this resulted in material with ~7.5% Sr and a room temperature absorption edge of about 0.5 eV. A 10-nm-thick PbSe capping layer was grown on the top of MQW structures to reduce strontium oxidation. Detailed procedures for CaF_2, BaF_2, and PbSe/PbSrSe epilayer growth on (111)-oriented silicon substrates are described in Ref. 2.

For the growth of PbSe/PbSrSe MQW structures on freshly cleaved BaF_2(111), a 100-nm-thick BaF_2 buffer layer was first grown on the substrate at 500 °C. Then the substrate temperature was reduced to 360 °C to grow the MQW structures. Detailed descriptions of PbSe/PbSrSe MQW growth on BaF_2(111) substrates are described in Ref. 4.

B. Structural and optical characterizations

MBE growth was monitored *in situ* using the RHEED technique. *Ex situ* structural characterization of the epilayers was performed using a Philips high-resolution x-ray diffraction system with four-crystal Ge(220) monochromator. Optical properties of the MQWs were studied by both FTIR transmission spectroscopy and midinfrared photoluminescence. To suppress unwanted Fabry–Perot interference fringes superposed on FTIR transmission spectra, the top surface of MQW samples was coated with a NiCr antireflection film.[5] A Biorad (FTS-60) FTIR spectrometer was used to measure transmission as a function of photon energy over a 700–6000 cm^{-1} spectral range. Sample temperature was varied from 4.2 to 300 K. FTIR transmission spectra were plotted as differential transmission ($\Delta T/T$) by subtraction of two spectra with only a few-degree temperature different to enhance absorption features. These differential spectra were made possible by the fact that the band gaps of IV–VI semiconductors are very sensitive to temperature variations.

PL measurements were performed by illuminating the MQW sample surface with a near-infrared (IR) diode laser with emission at 976 nm. A modular FTIR spectrometer (Oriel, MIR8000) and a liquid nitrogen cooled HgCdTe detector with a cutoff wavelength of 16 μm and a detectivity in the 3–4 μm range of about 2×10^{10} cm $Hz^{1/2}$/W were used to measure PL for various heat sink temperatures and pumping diode laser power density. MBE samples were clipped on a copper plate which was mounted on a single stage thermoelectric cooler. Diode laser radiation was unfocused and normally incident on epilayer surface with a spot area of about 6 mm^2. MQW luminescence was observed in a through-the-substrate geometry, which is possible due to the midinfrared transparency of both BaF_2 and Si substrates. More detailed description of PL measurements were given in Ref. 1.

III. RESULTS AND DISCUSSION

A. RHEED

Figure 1 shows the RHEED patterns during the growth of $BaF_2/CaF_2/Si(111)$ and PbSe/PbSrSe/BaF_2. The smooth transition from Si(111)-7×7 (a) to the CaF_2(111)-(1×1) (b) surface reconstruction provides evidence that CaF_2 growth on Si(111) proceeds via a two-dimensional (2D) Frank–van-Merwe growth mode. Continued 2D growth of BaF_2 on CaF_2 is confirmed by comparing (b) to (c). The growth of Pb(Sr)Se on BaF_2(111) substrates (d) and on $BaF_2/CaF_2/Si(111)$ proceeds first in a three-dimensional Volmer–Weber growth mode due to the higher (111) free surface energy of PbSrSe as compared to BaF_2. The spotty RHEED pattern (e) confirmed this growth mode. As the PbSrSe coverage increases to approximately 10 nm, the spotty RHEED pattern was gradually replaced by (1×1) streaks (f), indicating coalescence of surface islands and formation of a continuous layer. The PbSe/PbSrSe MQW samples grown on both BaF_2(111) and Si(111) substrates have mirror-like and crack-free surfaces. It is believed that lattice mismatch and thermal mismatch strain is relieved by dislocation glide through the fluoride and Pb(Sr)Se epilayers and that the resulting plastic deformation prevents crack formation.[6]

B. HRXRD

Figure 2 shows x-ray diffraction rocking curves for PbSe/PbSrSe MQW structures on both Si(111) (a) and BaF_2(111) (b) substrates. Both MQW samples have the same well width of 10 nm and barrier width of 50 nm. However, the sample grown on Si(111) has a 20 period MQW structure, while the sample grown on BaF_2(111) has a 40 period MQW structure. Satellite diffraction peaks with the order up to 5 from the MQW sample grown on Si were clearly seen, as compared to up to seven satellite peaks from the MQW sample grown on BaF_2. Spacings between satellite peaks were used to calculate QW thicknesses for each sample. The broader linewidth and fewer satellite peaks for the layers grown on Si(111) indicates poorer material quality likely due to the larger lattice mismatch (14%) and larger thermal expansion mismatch (700%) between the Pb(Sr)Se epilayers and the Si substrate thus causing more plastic deformation.

C. Midinfrared photoluminescence

Figures 3 and 4 show PL spectra from IV–VI MQW structures with different quantum well widths on both silicon and BaF_2 substrates at a heat sink temperature of 25 °C, for a pumping laser power density of 8.2 W/cm^2. Multiple peaks between 275 and 450 meV are observed from each sample. This is luminescence from the MQW modulated by Fabry–Perot interference inside the high refractive index ($n\sim5.4$) IV–VI layer. The Fabry–Perot cavity is formed by all epilayers in samples. Calculation of epilayer thicknesses from peak separations shown in Figs. 3 and 4 is in good agreement with that measured from x-ray diffraction. These interference fringes are typically observed in other measured optical spectroscopies, such as FTIR transmission,[7] reflection, and photoconductivity.[8] PL intensities measured from the MQW samples grown on Si substrates are weaker than those measured from the samples grown on BaF_2 substrates and

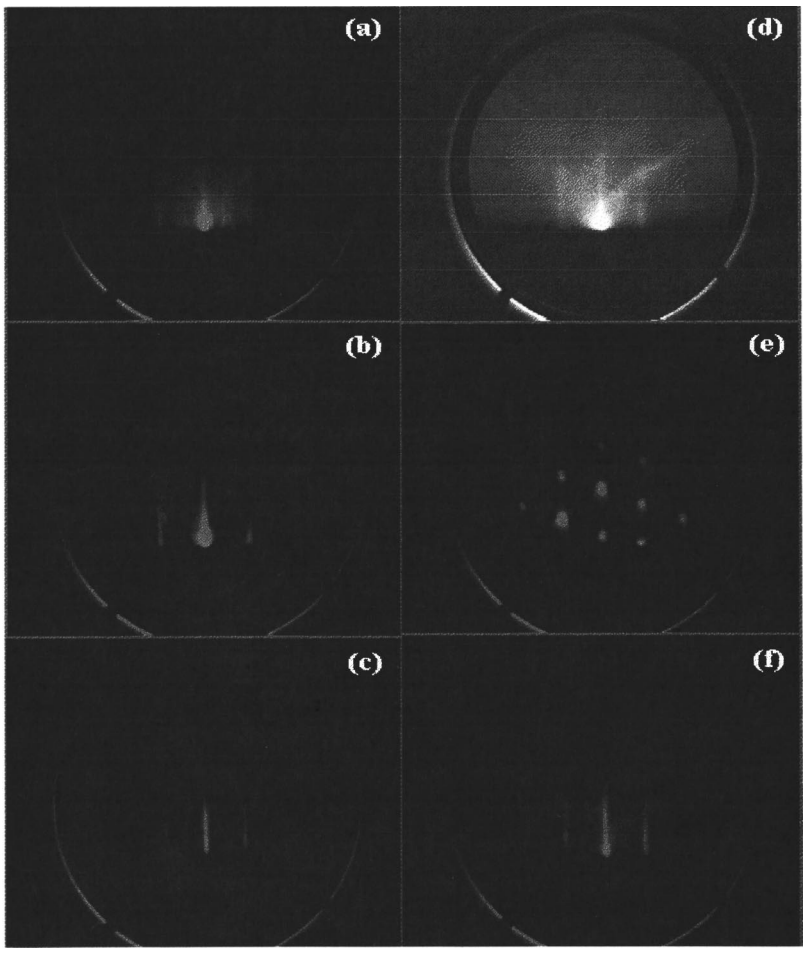

FIG. 1. RHEED patterns recorded at $[1\bar{1}0]$ azimuth: (a) Si(111) (7×7) after desorption of a hydrogen-terminated passivation layer at 700 °C; (b) after growth of 2 mm of CaF_2 on Si(111); (c) after growth of 600 nm of BaF_2 on CaF_2/Si(111); (d) BaF_2(111) substrate (1×1) at 500 °C; (e) after initial growth of 6 Å of PbSrSe on BaF_2; and (f) after growth of 3 μm of PbSrSe on BaF_2.

they are plotted on different scale in Figs. 3 and 4. The contrast of the interference fringes in the spectra for samples grown on Si is not as pronounced as that observed in the spectra for the samples grown on BaF_2 substrates. The reason is the much smaller refractive index difference between the IV–VI material ($n\sim5.4$) and silicon ($n=3.42$) as compared to BaF_2 ($n=1.45$). PL peak energies obtained from Gaussian fits, dotted lines in Figs. 3 and 4, increase as quantum well width decreases because of the quantum size effect. Figure 5 shows PL spectra measured from two samples on different substrates at a constant heat sink temperature of 25 °C and various pumping laser power densities. Figure 5(a) shows the spectra from a 40 pair MQW sample with well width of 210 Å grown on Si(111) and Fig. 5(b) shows the spectra from a 40 pair MQW sample with well width of 290 Å grown on BaF_2(111). Increasing pumping laser power density resulted in blueshifts of the PL emission in both samples. In Fig. 5(a), Gaussian fitted PL peak energies shifted from 305.5 to 322.4 meV as the pumping laser power density was increased from 2.8 to 13.6 W/cm^2. This increase in PL peak energies is due to localized heating of the IV–VI material associated with the higher photon flux from the near-IR laser. The blueshifts are much larger for the MQW sample grown on the BaF_2 substrate. Gaussian fitted PL peak energies shifted from 310.3 to 335.1 meV though the change in pump laser current was less (from 3.7 to 9.1 W/cm^2). The reason of the larger blueshift observed in the sample grown on BaF_2 is due to the much lower thermal conductivity of BaF_2 (11.7 $\mathrm{W\,m^{-1}\,K^{-1}}$) as compared to Si (150 $\mathrm{W\,m^{-1}\,K^{-1}}$). This heating effect will be discussed further in Sec. III E.

D. Differential transmission spectra

From the earlier PL measurements we have seen two effects: (1) interference fringes superposed on luminescent emission; (2) blueshifts of the PL peaks due to localized heating in the epilayers. These two effects make it difficult to understand the quantum state transitions involved in the PbSe/PbSrSe MQWs, which is important for design and fabrication of the midinfrared laser diodes using these materials. Several groups have contributed to the understanding of the fundamental problem using different optical techniques, such as transmission,[7,8] photoluminescence,[1] reflection, and photoconductivity.[8] However, in all the reports on band structure of IV–VI MQWs, optical spectra (transmission, reflection, photoluminescence, and photoconductivity) were superposed with strong interference fringes because of the high refractive index contrast between IV–VI materials and the growth substrates. Intersubband transitions in IV–VI MQWs could thus not be observed directly. Likewise the existence of interference fringes in PL spectra (shown in

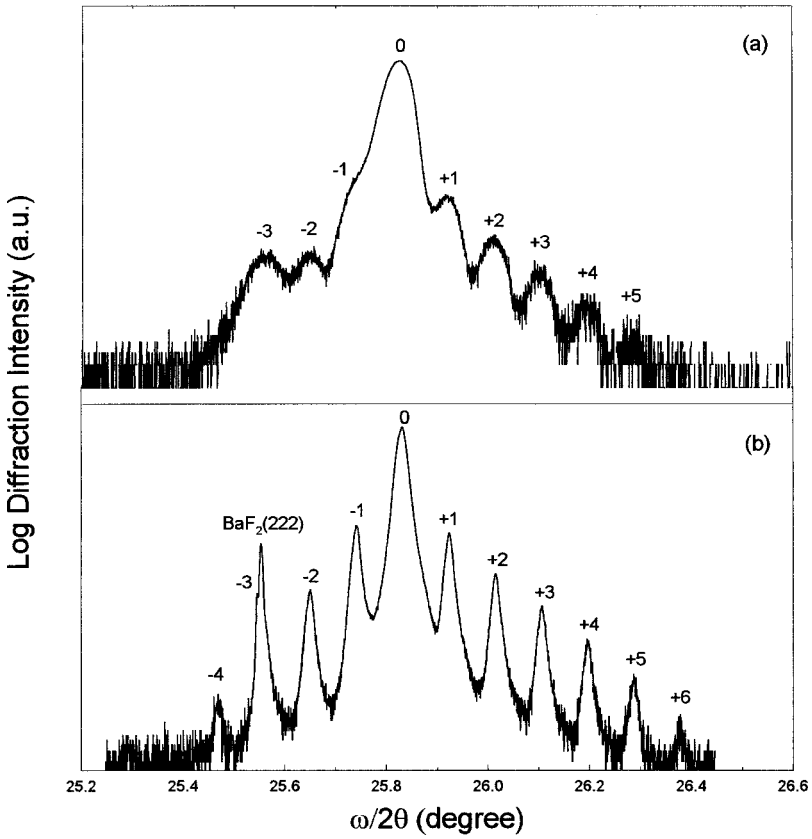

FIG. 2. High-resolution x-ray diffraction rocking curves for PbSe(10 nm)/PbSrSe(50 nm) MQW samples: (a) 20 period MQW structure grown on Si(111); and (b) 40 period MQW structure grown on BaF_2(111).

Figs. 3–5) makes it difficult to determine precisely the subband transition energies for the MQW samples studied here. Up until now, the study of electronic band structures of IV–VI MQWs has not been as satisfactory as that of III–V quantum wells.[9]

Figure 6 shows the low temperature differential transmission spectra of three MQW samples with different well widths, 29.7, 20.6, and 9.7 nm, respectively. Sr composition in PbSrSe barriers of the three MQW samples is kept the same, 7.5%. The barrier absorption edge is 405 meV. It is seen that the interference fringes are completely removed in these spectra. The attribution of the peaks is given in the figure. Unlike III–V materials, the band gap in IV–VI materials occurs at the L point in the Brillouin zone. Since the L

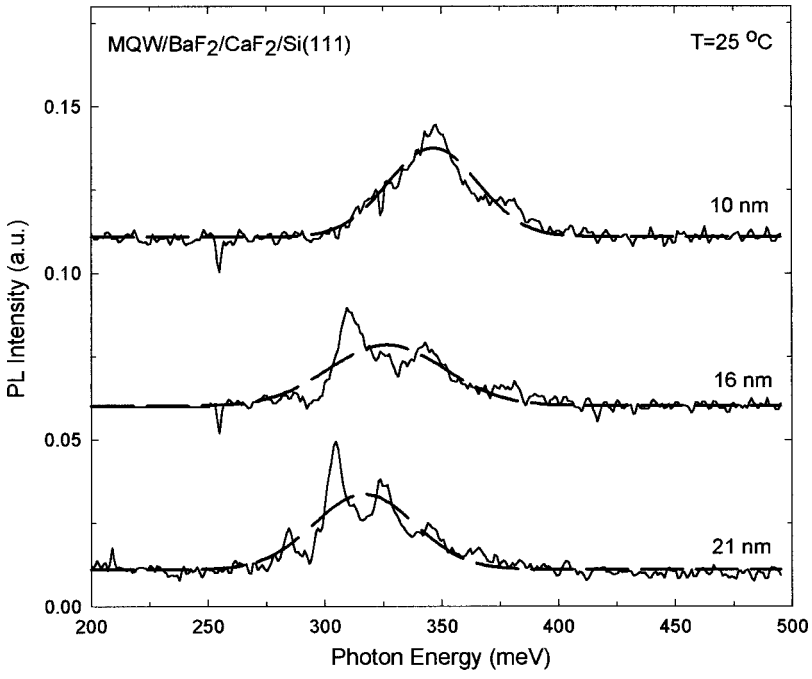

FIG. 3. Photoluminescence spectra for a heat sink temperature of 25 °C from three PbSe/PbSrSe MQW samples grown on Si(111) with a 600 nm BaF_2 buffer layer at a pumping laser power density of 8.2 W/cm^2. Gaussian fits of the PL peak energies are shown as dashed lines.

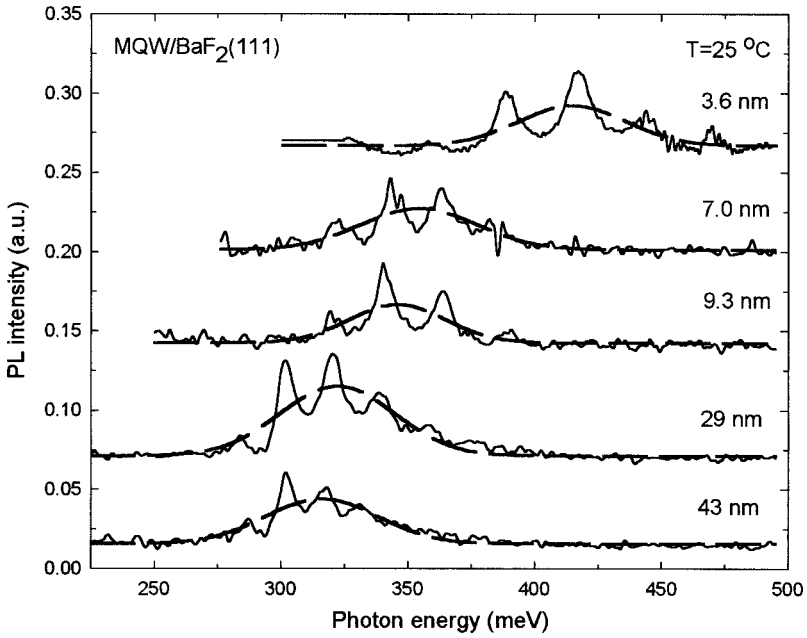

FIG. 4. Photoluminescence spectra for a heat sink temperature of 25 °C from five PbSe/PbSrSe MQW samples grown on $BaF_2(111)$ substrates at a pumping laser power density of 8.2 W/cm^2. Gaussian fits of the PL peak energies are also shown.

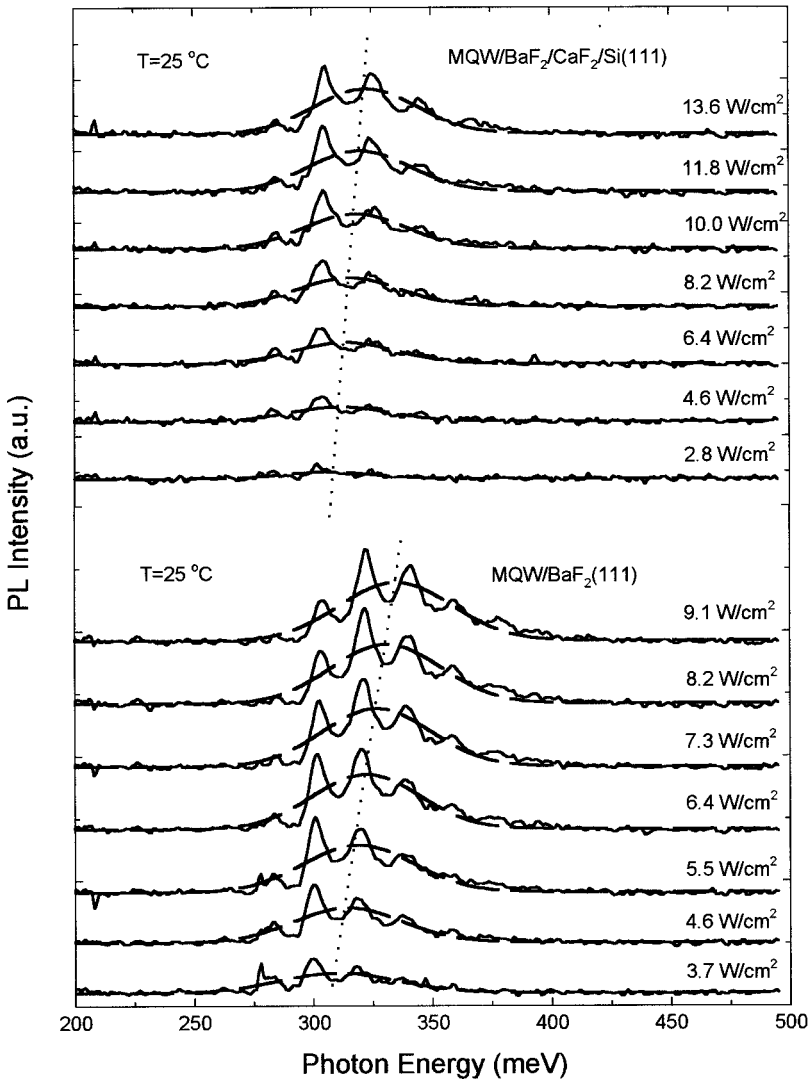

FIG. 5. Photoluminescence spectra for different pumping laser power densities and a constant heat sink temperature of 25 °C: (a) a 40 period PbSe(29 nm)/PbSrSe(50 nm) MQW sample grown on Si(111); and (b) a 40 period PbSe(21 nm)/PbSrSe(40 nm) MQW sample grown on $BaF_2(111)$ substrate. Gaussian fits of the PL peak energies are also shown.

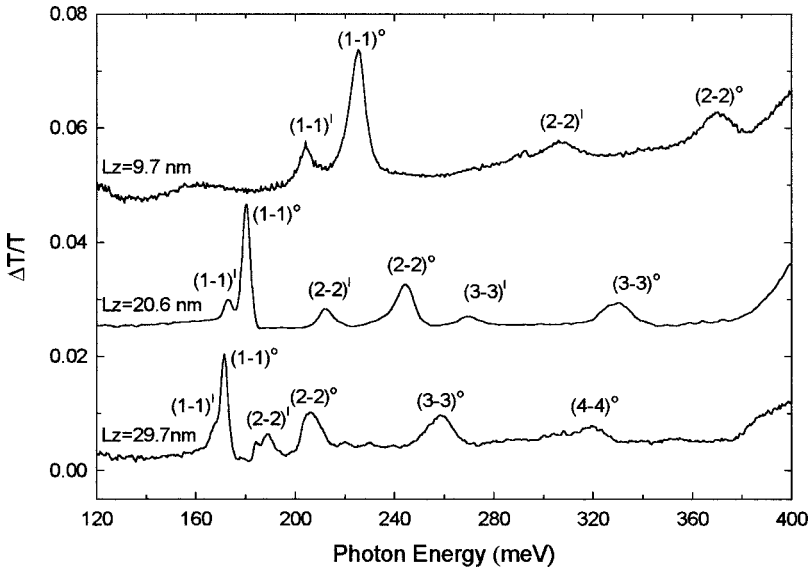

FIG. 6. FTIR differential transmission spectra of three MQW samples with well widths of 29.7, 20.6, and 9.7 nm, respectively. As well width decreases the $(i-i)^l$ and the $(i-i)^o$ transitions shift to higher energies and the number of confined states decreases.

point is four-fold degenerate, there will be four possible transitions. IV–VI layers grown on (111)-oriented substrates will thus have three $[11\bar{1}]$ valleys (oblique valleys) and one [111] valley (longitudinal valley). Oblique valleys have smaller effective electron and hole masses than the longitudinal valley.[10] According to quantum size effect, the longitudinal valley will have lower transition energy, while the three oblique valleys will have higher transition energies. The subband structures of IV–VI MQWs were calculated by Kriechbaum *et al.*[11,8] As shown in Fig. 6, longitudinal-valley subband transitions $(i-i)^l$ and oblique-valley transitions $(i-i)^o$ are clearly resolved in all three MQW samples. As the well width decreases from 29.7 to 9.7 nm, the splitting between the $(1-1)^l$ transition and the $(1-1)^o$ transition increases from 4 to 20 meV, due to the quantum size effect. As expected, the number of subbands involving both longitude and oblique valleys decreases from 4 to 2. It is noted that the differential transmission spectra shown in Fig. 6 are dominated by oblique-valley subband transitions. A comparison of the integrated intensity difference between $(i-i)^l$ and $(i-i)^o$ reflects the difference in the density of states related to the two different valleys. The joint density of states and the transition matrix elements of oblique valleys with their three-fold degeneracy are larger than those of the longitudinal valley, and as a consequence the observed intensities of the $(i-i)^o$ transitions are higher than that of the $(i-i)^l$ transitions. As temperature increases, all the subband transitions and barrier continuum move to higher energies, and peaks broaden due to increased phonon scattering.

Figure 7 shows the comparison of the transmission measurements with the calculations using the envelope wave function approximation. In PbSe/PbEu(Sr,Mn)Se MQW systems a type I transition alignment was shown at low Eu(Sr,Mn) concentrations. An equal band offset for conduction band and valence band of the PbSe/PbSrSe MQW, $\Delta E_c:\Delta E_v=1:1$, was used. The band structure parameters for the calculations of quantized states of electrons and holes are from Ref. 10. The barrier heights were taken from measured FTIR transmission spectra. The calculations presented in Fig. 7 only contain the quantum size effect, which is the dominant contribution in the case of these MQW structures. Strain-induced shifts of transition energies in the PbSe well layers are not considered here. The lattice mismatch between $BaF_2(111)$ and the epilayer is ~1% at room temperature. The epilayer thickness is ~0.8 μm. Thus, it is expected the PbSe/PbSrSe epilayers are relaxed. However, the lattice mismatch between PbSe wells and PbSrSe barriers is small, 0.18%, and the resulting elastic misfit strain leads to a tensile strain in PbSe and to a compressive strain in the PbSrSe layers. In these MQW samples it is expected the total strain is shared between PbSe well layers and PbSrSe barrier layers. Theoretical calculations showed the tensile strain in PbSe quantum well layers would also cause the splitting of the degeneracy of the longitudinal valley and oblique valleys by a few milli-electron-volts.[11] Reliable shear deformation potential values are not available, so it is outside the scope of this article to evaluate this further. Other effects such as the exciton energy in PbSe are estimated to be small (<1 meV) and can be neglected in this analysis.

Comparing the calculations (lines) with the measured $(1-1)^l$ and $(1-1)^o$ transition energies at 4.2 and at 295 K shown in Fig. 7, it is clear that the calculations give a good description of the well width dependence of the optical transitions in the PbSe/PbSrSe MQWs. In the room temperature transmission spectra, due to phonon-scattering broadening of the subband transitions involving both of longitudinal and oblique valleys, $(1-1)^l$ and $(1-1)^o$ could not be resolved. Therefore, the experimental points represent the combination of ground state transitions from both valleys.

E. Heating effect in epilayers

Compared to room temperature ground state transition energies shown in Fig. 7 (no heating effect involved), the PL emission energies shown in Fig. 5 are shifted to significantly higher ones as pumping laser power density increases. This

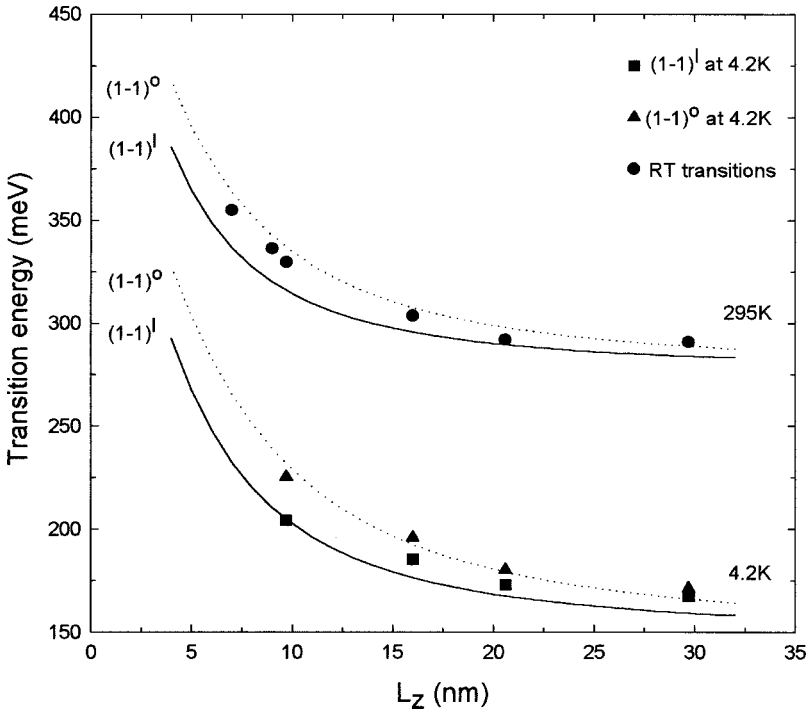

FIG. 7. Transition energies as a function of the well width for the PbSe/PbSrSe MQWs at 4.2 and 295 K. Transition energy calculations using the envelope wave function approximation are plotted as solid lines. The experimental points are from the FTIR measurements, ■ $(1-1)^{l}$ at 4.2 K, ▲ $(1-1)^{o}$ at 4.2 K, and ● the room temperature transition energies.

comparison allows quantitative evaluation of localized heating due to increasing photon flux from the pumping laser. The ground state energies measured from FTIR transmission as shown in Fig. 7 are not significantly affected by heating from the low intensity broadband blackbody source used in the FTIR instrument. In contrast, localized temperature in epilayers illuminated with a high intensity laser can be much higher than the heat sink temperature because of photon-phonon or excited-electron-phonon scattering and the low thermal conductivity of the IV–VI and/or substrate materials. For the sample grown on $BaF_2(111)$, the luminescent peak shifts from 310.3 to 335.1 meV as the near-IR laser power density increases from 3.7 to 9.1 W/cm^2. If there were no heating effect the PL peak should be at 291 meV as given by both measurement and calculation in Fig. 7. Using the 0.51 meV/K temperature-tuning coefficient for PbSe (100–400 K),[10] the localized temperature in the epilayers is determined to be as high as 108 °C, 83 °C higher than the heat sink temperature, for the 9.1 W/cm^2 pumping laser power

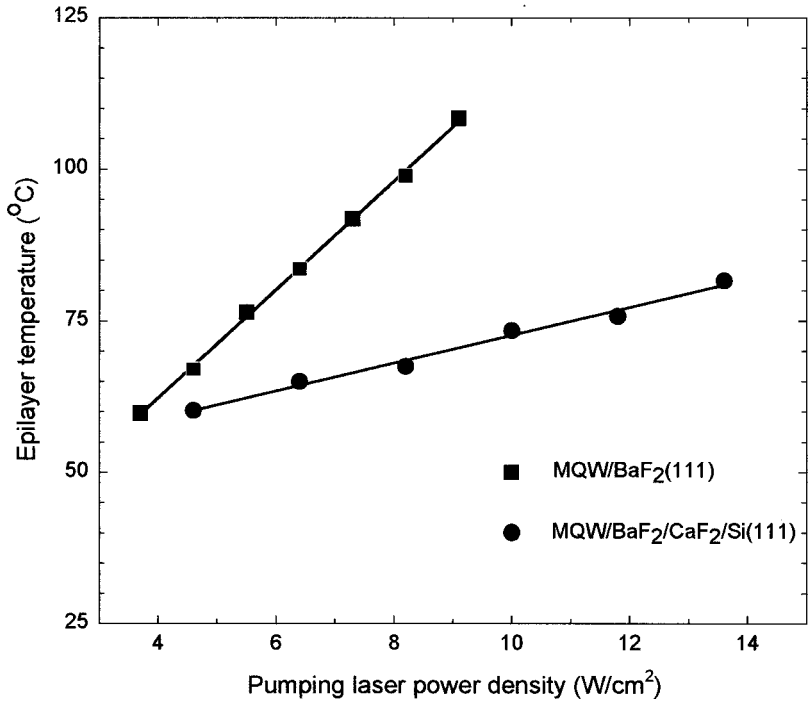

FIG. 8. Epilayer temperature rise due to increasing photon flux from near-IR pumping laser. ● the 40 period PbSe(29 nm)/PbSrSe(50 nm) MQW grown on $BaF_2/CaF_2/Si(111)$; ■ the 40 period PbSe(21 nm)/PbSrSe(40 nm) MQW grown on $BaF_2(111)$.

density. For samples grown on Si the heating effect is much less. The luminescent peak shifts from 305.5 to 322.4 meV as the near-IR laser current increases from 2.8 to 13.6 W/cm^2. At a pumping laser power density of 9.1 W/cm^2, the PL peak energy is 317.5 meV. This peak energy corresponds to a localized temperature of 70 °C, 45 °C higher than the heat sink temperature. Clearly, the higher thermal conductivity of the silicon substrate compared to that of BaF_2 improves heat dissipation from the IV–VI layers, and this reduces the amount of localized heating due to photon-phonon or excited-electron-phonon scattering associated with the incident 1.27 eV near-IR excitation photons (Fig. 8).

It is noted that in the as-grown samples on Si(111) a 600-nm-thick buffer layer between Si substrate and PbSe/PbSrSe MQW was grown. Growth of such structures allows removal of the silicon growth substrate by dissolving the BaF_2 buffer layer in water and transfer of the IV–VI layers to more thermally conductive substrates such as copper.[12,13] The epilayers are quite robust, and after transfer of epilayers PL emission can still be observed. In addition, degradation in PL intensity has not been observed either due to testing or storage in laboratory air. The ability to obtain midinfrared emission for a variety of different test conditions and from a variety of different structures grown on silicon shows that these materials have promise for relatively easy fabrication of reliable luminescent devices.

IV. CONCLUSION

High quality PbSe/PbSrSe MQW structures were grown on Si(111) and BaF_2(111) substrates by MBE. Experimental demonstration of PL emission from both sets of MQW samples has been described and longitudinal-valley and oblique-valley subband transitions without superposed interference fringes were unambiguously revealed for the first time by FTIR differential transmission spectroscopy. The differential transmission spectra of the MQW structures directly show the unique band structure of IV–VI semiconductors: the quantum size effect split the four-fold degeneracy at *L* point of both conduction band and valence band into a singlet longitudinal valley and triplet oblique valleys. So in addition to strong QW hole confinement and reduced Auger recombination, transitions between low-density of states longitudinal valleys may be a key factor in obtaining the remarkable PL results. Furthermore, the combination of the FTIR differential transmission and PL spectra allows precise determination of localized heating in the MQW samples due to increasing optical pumping levels. The MQW samples grown on Si show significantly less epilayer heating than similar structures grown on BaF_2 substrates. These measurements provide a way to quantify localized heating in an epitaxially grown layer. Results have shown the role of higher substrate thermal conductivity in enhancing heat dissipation from the optically active material.

ACKNOWLEDGMENTS

P. H. O. Rappl would like to acknowledge the financial support from Fundaçao de Amparo à Pesquisa do Estado de Sào Paulo-Fapesp, Proc: 00/02415-3. This work was supported by a grant from NSF No. DMR-9802396.

[1]P. J. McCann, K. Namjou, and X. M. Fang, Appl. Phys. Lett. **75**, 3608 (1999).
[2]P. J. McCann, X. M. Fang, W. K. Liu, B. N. Strecker, and M. B. Santos, J. Cryst. Growth **175/176**, 1057 (1997).
[3]A. Lambrecht, N. Herres, B. Spanger, S. Kuhn, H. Böttner, M. Tacke, and J. Evers, J. Cryst. Growth **108**, 301 (1991).
[4]X. M. Fang, K. Namjou, I. Chao, P. J. McCann, N. Dai, and G. Tor, J. Vac. Sci. Technol. B **18**, 1720 (2000).
[5]S. W. McKnight, K. P. Stewart, H. D. Drew, and K. Moorjani, Infrared Phys. **27**, 327 (1987).
[6]P. Müller, H. Zogg, A. Fach, J. John, C. Paglino, A. N. Tiwari, M. Krejci, and G. Kostorz, Phys. Rev. Lett. **78**, 3007 (1997).
[7]A. Ishida, S. Matsuura, M. Mizuno, and H. Fujiyasu, Appl. Phys. Lett. **51**, 478 (1987).
[8]S. Yuan, G. Springholz, G. Bauer, and M. Kriechbaum, Phys. Rev. B **49**, 5476 (1994); H. Krenn, S. Yuan, N. Frank, and G. Bauer, *ibid.* **57**, 2393 (1998).
[9]R. C. Miller, D. A. Kleinman, and A. C. Bossard, Phys. Rev. B **29**, 7085 (1984).
[10]Landolt–Börnstein, in *Numerical Data and Functional Relationships in Science and Technology*, Non-Tetrahedrally Bonded Compounds Vol. 17, edited by O. Madelung (Springer, Berlin, 1987).
[11]M. Kriechbaum, K. E. Ambrosch, E. J. Fantner, H. Clemens, and G. Bauer, Phys. Rev. B **30**, 3394 (1984).
[12]H. Z. Wu, X. M. Fang, R. Salas, D. McAlister, and P. J. McCann, Thin Solid Films **352**, 277 (1999).
[13]M. F. Khodr, P. J. McCann, and B. A. Mason, IEEE J. Quantum Electron. **94**, 1604 (1998).